Effects of Ti additive on the structure and electrochemical performance of $LiMnPO_4$ cathode material

Laifen Qin[a,b], Yonggao Xia[a,*], Hailiang Cao[a], Linjun Luo[a], Qian Zhang[a], Lipeng Chen[a], Zhaoping Liu[a,*]

[a] *Ningbo Institute of Materials Technology Engineering (NIMTE), Chinese Academy of Sciences, Zhejiang, 315201, P. R. China*
[b] *The Faculty of Science, Ningbo University, Zhejiang, 315211, P. R. China*

ARTICLE INFO

Keywords:
Lithium ion batteries
Cathode material
Lithium manganese phosphate
Electrochemical performance

ABSTRACT

The (1-x)$LiMnPO_4$·$Li_xTi_x(PO_4)_\delta$ (x = 0, 0.01, 0.05, 0.10, 0.15, 0.20) cathode materials are successfully synthesized through a solid-state method. The structures and electrochemical properties of the prepared samples have been characterized comprehensively. It is found minority phases containing $LiTi_2(PO_4)_3$ and TiP_2O_7 were formed. The addition of Ti has obviously reduced the size of grains. Electrochemical tests indicate that the discharge capacities of $LiMnPO_4$ samples can be significantly improved with the addition of Ti. Especially, the (1-x)$LiMnPO_4$·$Li_xTi_x(PO_4)_\delta$ sample with x = 0.1 has the largest discharge specific capacity, which is more than 131 mAh g^{-1} at 0.05 C. And EIS tests[1]demonstrate that the 0.9$LiMnPO_4$·$Li_{0.1}Ti_{0.1}(PO_4)_\delta$ sample has lower charge transfer resistance and higher diffusion coefficient than the pristine $LiMnPO_4$ sample.

1. Introduction

Olivine lithium transition-metal phosphates $LiMPO_4$ (M = Fe, Mn, Co and Ni), which are firstly reported by Padhi and Goodenough et al., have been intensively studied in the past few years [1–3]. The presence of the strong covalently-bonded PO_4^{3-} tetrahedral polyanion in the olivine structure can stabilized the three-dimensional (3D) framework, thus giving rise to good cycling performance and excellent thermal stability of $LiMPO_4$ cathode materials [4]. In this family of phosphates, $LiMnPO_4$ has higher Li^+ intercalation potential of 4.1 V versus Li^+/Li and the theoretical energy density (701Wh kg^{-1}) is 1.2 times larger than that of commercialized $LiFePO_4$ (578Wh kg^{-1}). Moreover, the 4.1 V intercalation potential of $LiMnPO_4$ is compatible with present non-aqueous organic electrolytes of lithium ion batteries.

Unfortunately, some intrinsic disadvantages hinder $LiMnPO_4$ from its practical applications in lithium ion batteries. Because of the heavy polaronic holes localized on the Mn^{3+} sites (the Jahn-Teller ion) and the interfacial strain between the $LiMnPO_4$ and $MnPO_4$ phase, $LiMnPO_4$ is subjected to poorer electronic conductivity and lower lithium diffusivity than those of $LiFePO_4$ [5–7]. Consequently, these drawbacks result in its low discharge capacity, high polarization and poor rate capability.

Recently, many attempts have been made to improve the electrochemical performance of $LiMnPO_4$ cathode materials, such as carbon coating [8–10], particle size reduction and morphology control [11–14]. In addition, several groups have found that cation doping or substitution is an effective way to enhance the electrochemical performance [15–20]. For example, Wang et al. [15] investigated the properties of the cation substituted $LiMn_{0.9}M_{0.1}PO_4$ (M = Fe, Ni, Mg, Zn), and the optimum performance improvement was achieved by Fe substitution. Hong et al. [16] synthesized a series of nanoporous $LiFe_xMn_{1-x}PO_4$ compounds (with x = 0, 0.05, 0.1, 0.15, and 0.2), and found $LiFe_{0.2}Mn_{0.8}PO_4$ showed the best electrochemical performance among all samples. Fang et al. [17] studied the effect of Zn doping, and a specific discharge capacity as high as 139 mAh g^{-1} at 0.1 C could be obtained for $LiMn_{0.98}Zn_{0.02}PO_4$, but a too high level of Zn doping would reduce the reversible capacity of the material. From above results, it is confirmed that the electrochemical performance of $LiMnPO_4$ cathode materials strongly depends on the rational cation substitution and the doping content.

More recently, we note that many researchers have reported doping a small amount of Ti into $LiFePO_4$ can significantly enhance its electrochemical performance [21–23]. Under the inspiration of these successes of $LiFePO_4$, it is speculated that it would be possible to synthesize Ti additive $LiMnPO_4$ with the greatly enhanced electrochemical performance. However, Shiratsuchi et al. [18] found that the performance of the sample with 1% Ti doping can't be improved well compared with the undoped sample. We doubt that

* Corresponding author. Tel.: +86 574 8668 5096; fax: +86 574 8668 5096.
E-mail addresses: xiayg@nimte.ac.cn (Y. Xia), liuzp@nimte.ac.cn (Z. Liu).

the Ti doping level (x = 0.01) is so little that it doesn't demonstrate the effect of Ti doping exactly and determine whether or not high Ti additive would enhance performance in their experiment.

In this paper, to study the effect of Ti additive and find the optimum addition level, Ti additive $LiMnPO_4$ materials were synthesized through solid-state method. In the synthesis process, glucose was used as carbon source and reduction agent. We refer to the resulting materials as (1-x)$LiMnPO_4$·$Li_xTi_x(PO_4)_\delta$ in this manuscript. The physical and electrochemical properties of the materials have been investigated systematically in detail.

2. Experimental

2.1. Preparation

$CH_3COOLi{\cdot}2H_2O$, $NH_4H_2PO_4$, $(CH_3COO)_2Mn{\cdot}4H_2O$, TiO_2 nanopowders and glucose (10 wt% of the product mass) in a stoichiometric ratio of Li:(Fe/Ti):P = 1:1:1 were mixed with an appropriate amount of ethanol and ground for 6 h in a planetary ball mill under the rotation speed of 350 rpm. After that, the mixture was dried at 80°C to evaporate the ethanol, then collected and heated to 600°C in argon atmosphere at a heating rate of 5°C min^{-1}; it was sintered for 4 h to obtain the (1-x)$LiMnPO_4$·$Li_xTi_x(PO_4)_\delta$ (x = 0, 0.01, 0.05, 0.10, 0.15, 0.20) samples.

2.2. Structure and morphology characterization

The crystalline structures of the samples were characterized by X-ray powder diffraction (XRD), using an AXS D8 Advance diffractometer with Cu Kα radiation. The morphologies and microstructures were observed by field emission scanning electron microscopy (SEM) (S-4800, Hitachi) and high-resolution transmission electron microscopy (HRTEM) (Tecnai F20, FEI). Elemental mapping was used to demonstrate the existence and distribution of composition elements in the as-prepared particles. The amount of Carbon was tested by using CHNS/O Elemental Analyzer (PE2400II, Perkin-Elmer). The electrical conductivity was measured by the four-point probe meter (CRESBOX, NAPSON)

2.3. Electrochemical measurements

Electrochemical properties of the (1-x)$LiMnPO_4$·$Li_xTi_x(PO_4)_\delta$ electrodes were measured through electrochemical cells assembled in an argon glove box. Firstly, the paste was prepared by mixing active material (80 wt.%), Super P carbon (SP, 15 wt.%) and poly(vinylidene fluoride) (PVDF, 5 wt.%)) in N-methyl-2 pyrrolidinone (NMP) solution and then coated on an Al foil using automatic film-coating equipment. After dried, pressed under 6 MPa, the resultant film was punched onto 13-mm diameter discs as cathode; lastly, the coin cells were assembled in an argon-filled glove box using Celgard 2502 as separator and lithium foil as anode. 1 M $LiPF_6$ (dissolved in ethylene carbonate and dimethyl carbonate with a 1:1 volume ratio) was employed as electrolyte. The coin-type cells were tested within a voltage range of 2.0-4.5 V using a constant-current-constant-voltage (CC-CV) protocol at various rates with potentiostatic steps at the cutoff potential on a cell testing system (LAND CT2001A, China). The cyclic voltammogram (CV) was performed between 2.0 V and 4.5 V using the Solartron 1400 cell test system with a scan rate of 0.1 mV s^{-1}. The electrochemical impedance spectroscopy (EIS) measurements were carried out in a frequency range from 0.01 Hz -100,000 Hz with a voltage amplitude of 5 mV using the same facility. All the EIS tests were measured on the cells after 3-cycles test at 0.1 C. All the specific capacity was determined by subtracting the mass of carbon added in synthesis of (1-x)$LiMnPO_4$·$Li_xTi_x(PO_4)_\delta$ series samples.

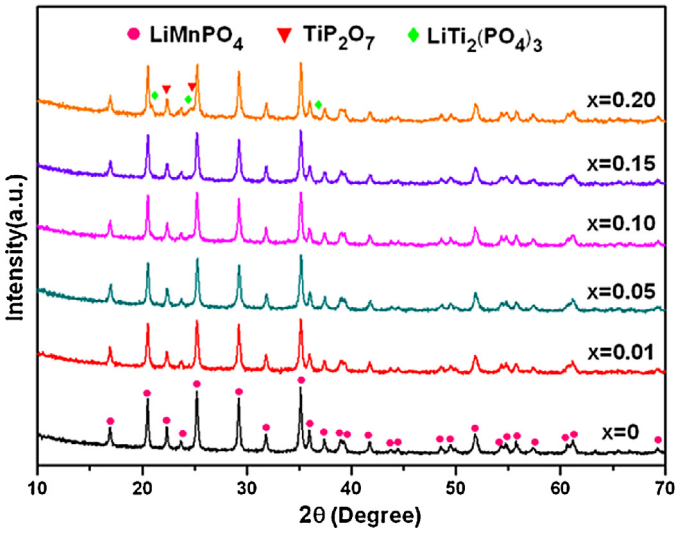

Fig. 1. XRD patterns of the as-prepared (1-x)$LiMnPO_4$·$Li_xTi_x(PO_4)_\delta$ samples.

3. Results and discussion

Fig. 1 shows the XRD patterns of the as-prepared (1-x)$LiMnPO_4$·$Li_xTi_x(PO_4)_\delta$ (x = 0, 0.01, 0.05, 0.10, 0.15, 0.20) series samples. For the pristine $LiMnPO_4$, all the diffraction peaks correspond well to the orthorhombic $LiMnPO_4$ phase with Pnmb space group (ICSD #25834). For the x = 0.2 sample, it can been seen that the phase peaks of $LiTi_2(PO_4)_3$ (ICSD #95979) and TiP_2O_7 (ICSD #279581) exist in the XRD patterns. However, there is no obvious diffraction peak of titanium phosphates in the samples with low content of Ti ($x \leq 0.15$).

The carbon contents of the as-prepared samples were tested by total organic carbon analysis and listed in Table 1. The carbon content of the x = 0 and 0.01 samples are little higher than others which result in higher electrical conductivities contributed by carbon. The others have almost identical carbon content. Hence the enhancement in electrical conductivity mostly attributes to the titanium additive. The bulk conductivity of Ti additive $LiMnPO_4$ can improve with increasing Ti content. It is obviously seen that the x = 0.10 sample has the largest conductivity. However, the conductivities of the x = 0.15 and 0.20 materials diminish, which may be due to the increase of $LiTi_2(PO_4)_3$ and TiP_2O_7 phases. Consequently, the proper Ti content can be beneficial to improve the electrochemical performance of the $LiMnPO_4$ cathode material.

Rietveld method was used to refine the X-ray diffraction patterns aiming to analyze the crystal structures of the samples, and the refined results are listed in Table 1. All the reliability factors (Rw) are less than 10%, indicating that the fitting results are good. As shown in Fig. 2, the x = 0.01 sample exhibits larger lattice volume values than the pure $LiMnPO_4$. This is possibly because some Ti^{4+} ions substitute Li^+ sites, since the ionic radius of Ti^{4+} in octahedral coordination (0.068 nm) is larger than the radius of Li^+ (0.061 nm). Further increasing the content of Ti, the lattice volume values reduce slowly. It is supposed that partial Ti^{4+} ions tend to substitute for Mn^{2+} on increasing the amount of Ti^{4+}. The lattice parameters can decline because the ionic radius of Ti^{4+} is smaller than that of Mn^{2+}. The result conforms to that reported by Chiang et al. [24], they suggest that Ti^{4+} ions may occupy M1 (Li^+) sites to form solid solutions without any impurity; or occupy M2 (Mn^{2+}) sites with some impurities.

Fig. 3 shows the SEM images of the (1-x)$LiMnPO_4$·$Li_xTi_x(PO_4)_\delta$ samples. All the samples have some degrees of agglomeration. Obviously, it can be observed that the Ti additive $LiMnPO_4$ samples have the smaller grain size and uniform size distribution with

Table 1
The lattice parameters, carbon contents and electrical conductivities of the as-prepared (1-x)$LiMnPO_4{\cdot}Li_xTi_x(PO_4)_\delta$ samples.

Sample	Lattice parameters				Rw(%)	Carbon Content(%)	Conductivity ($S\,cm^{-1}$)
	a(Å)	b(Å)	c(Å)	V($Å^3$)			
x = 0	6.1071	10.4529	4.7473	303.0529	5.92	2.76	2.9×10^{-5}
x = 0.01	6.1090	10.4551	4.7477	303.2366	5.12	2.75	4.76×10^{-5}
x = 0.05	6.1074	10.4522	4.7470	303.0284	5.47	2.38	4.44×10^{-5}
x = 0.10	6.1069	10.4533	4.7466	303.0099	6.79	2.35	1.90×10^{-4}
x = 0.15	6.1067	10.4526	4.7470	303.0052	6.87	2.32	3.29×10^{-5}
x = 0.20	6.1070	10.4514	4.7471	302.9917	8.23	2.40	5.43×10^{-5}

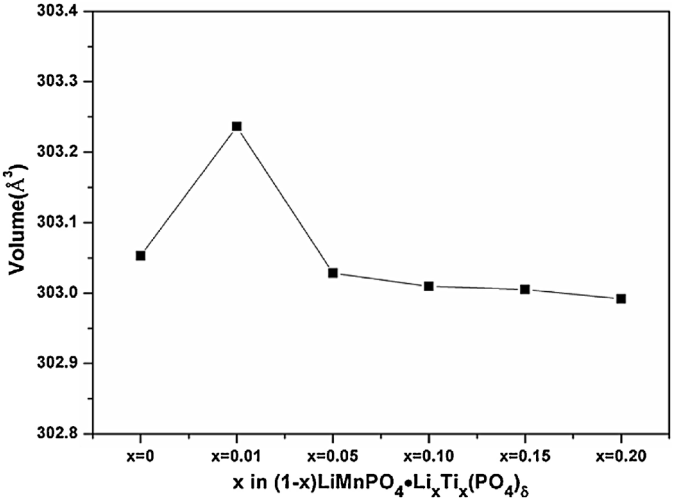

Fig. 2. The lattice volume of the (1-x)$LiMnPO_4{\cdot}Li_xTi_x(PO_4)_\delta$ samples.

increasing the content of Ti. The grain sizes of the pristine $LiMnPO_4$ are 50-400 nm (Fig. 3a). By comparison, the grain sizes of the sample with the highest Ti content (x = 0.20) are mostly 50-100 nm (Fig. 3f). The reduction of the grain size could shorten the lithium diffusion distance, which would enhance the electrochemical performance of the $LiMnPO_4$ cathode material. Besides, elemental mappings of PKα, OKα, TiKα, MnKα and CKα in Fig. 4 corresponding to $0.9LiMnPO_4{\cdot}Li_{0.1}Ti_{0.1}(PO_4)_\delta$ sample were analyzed. These micrographs indicate that all the component elements in the particles were equally distributed.

In order to precisely observe the phase compositions of the Ti additive samples, the $0.8LiMnPO_4{\cdot}Li_{0.2}Ti_{0.2}(PO_4)_\delta$ sample which has the high Ti content was used to test. TEM and HRTEM images of $LiMnPO_4$ and $0.8LiMnPO_4{\cdot}Li_{0.2}Ti_{0.2}(PO_4)_\delta$ samples are displayed in Fig. 5. As shown in Fig. 5a and c, the prepared particles have been uniformly coated with carbon. The thickness of carbon layer is about 2 nm. The carbon coating on the particles surface not only can prevent the particles from aggregating, but also can improve the electrical conductivity of the samples. HRTEM was used to further study the microstructure of the as-prepared products. In Fig. 5b, the pristine $LiMnPO_4$ sample exhibits regular lattice fringes of the (011) crystalline plane with measured d spacing value of 0.432 nm. For the $0.8LiMnPO_4{\cdot}Li_{0.2}Ti_{0.2}(PO_4)_\delta$ sample, two kinds of lattice fringes in Fig. 5d can be seen, one is the lattice fringe of $LiMnPO_4$ (interplanar spacing 0.352 nm, lattice plane (111)), the other is the lattice fringe of $LiTi_2(PO_4)_3$ (interplanar spacing 0.363 nm, lattice plane (113)). This further confirms that $LiTi_2(PO_4)_3$ phase exists in the Ti additive $LiMnPO_4$ samples.

The initial cyclic voltammogram curves of the samples between 2.0 and 4.5 V at a scan rate of 0.1 mV s^{-1} are depicted in Fig. 6. All the samples have well-defined symmetrical peaks. As for the pure $LiMnPO_4$ (x = 0), there is one redox potential peaks around 4.36/3.92 V, which accords with the phase transition $LiMnPO_4$ and $MnPO_4$. For the Ti additive $LiMnPO_4$ samples, other three redox couple peaks at 2.31/2.28 V, 2.43/3.2.41 V, 2.82/2.79 V can be seen.

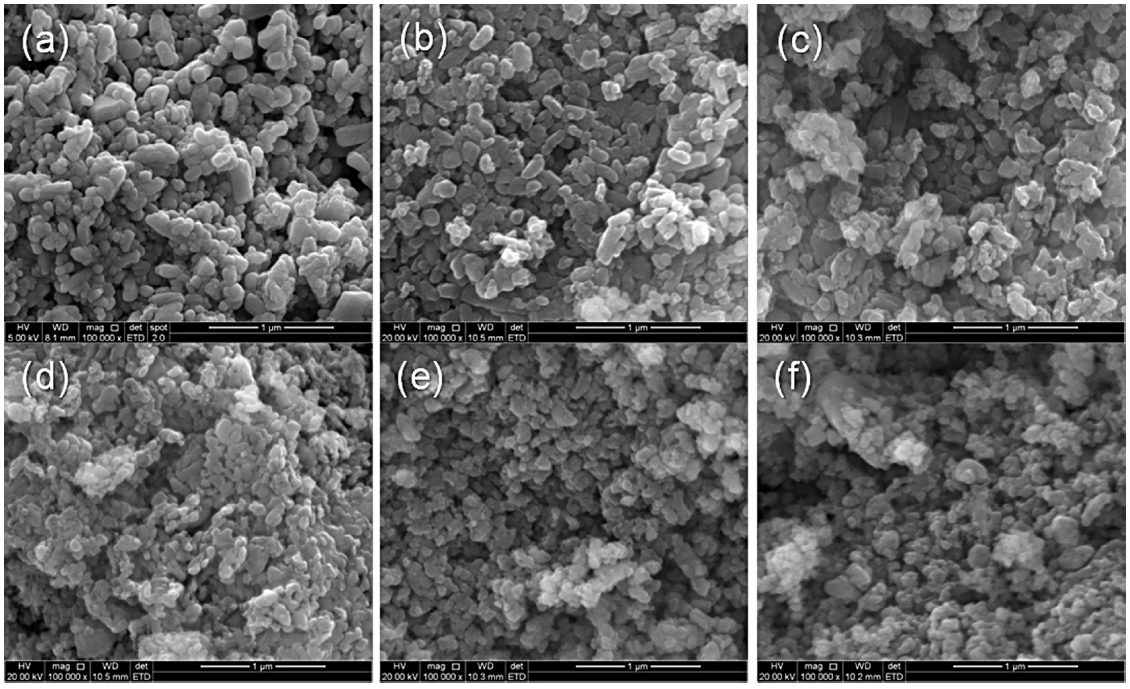

Fig. 3. SEM images of the (1-x)$LiMnPO_4{\cdot}Li_xTi_x(PO_4)_\delta$ samples: (a) x = 0, (b) x = 0.01, (c) x = 0.05, (d) x = 0.10, (e) x = 0.15, (f) x = 0.20.

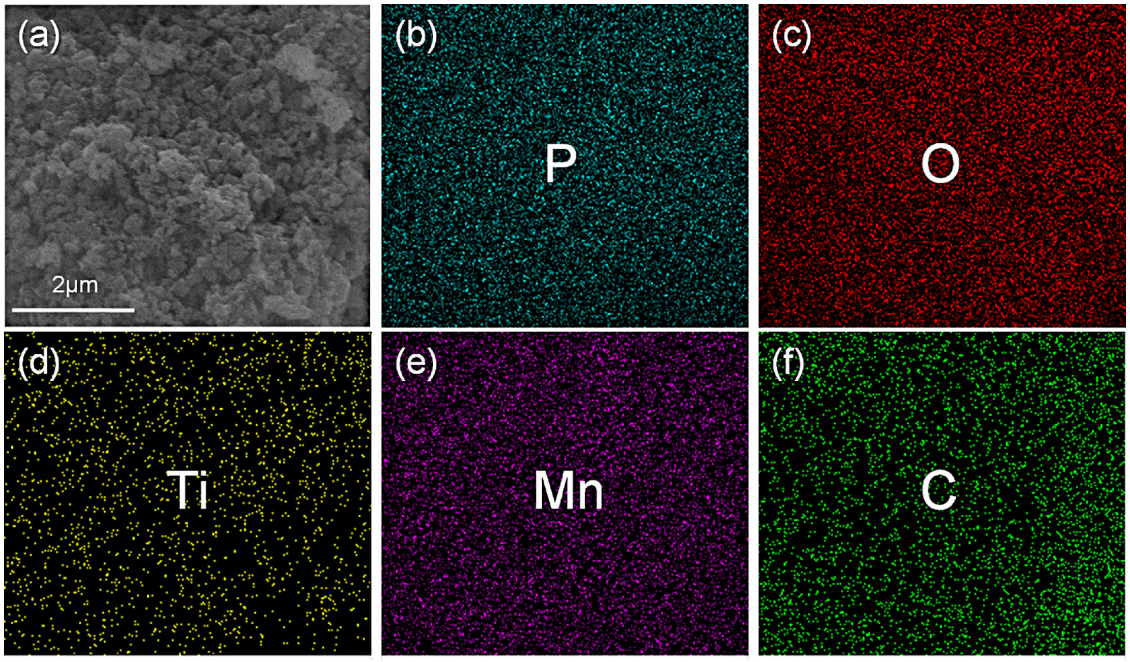

Fig. 4. (a) SEM image of $0.9LiMnPO_4{\cdot}Li_{0.1}Ti_{0.1}(PO_4)_\delta$ and elemental mappings for (b) P, (c) O, (d) Ti, (e) Mn, (f) C.

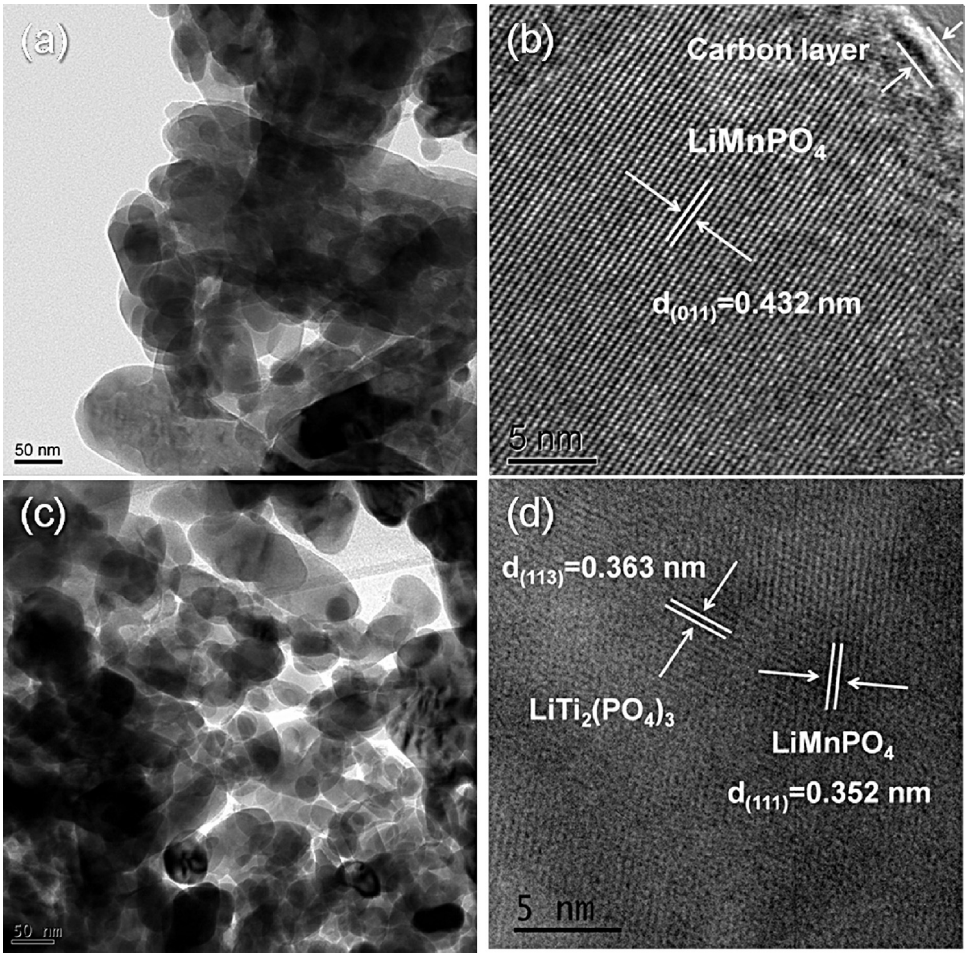

Fig. 5. TEM and HRTEM images of (a, b) $LiMnPO_4$ and (c, d) $0.8LiMnPO_4{\cdot}Li_{0.2}Ti_{0.2}(PO_4)_\delta$ samples.

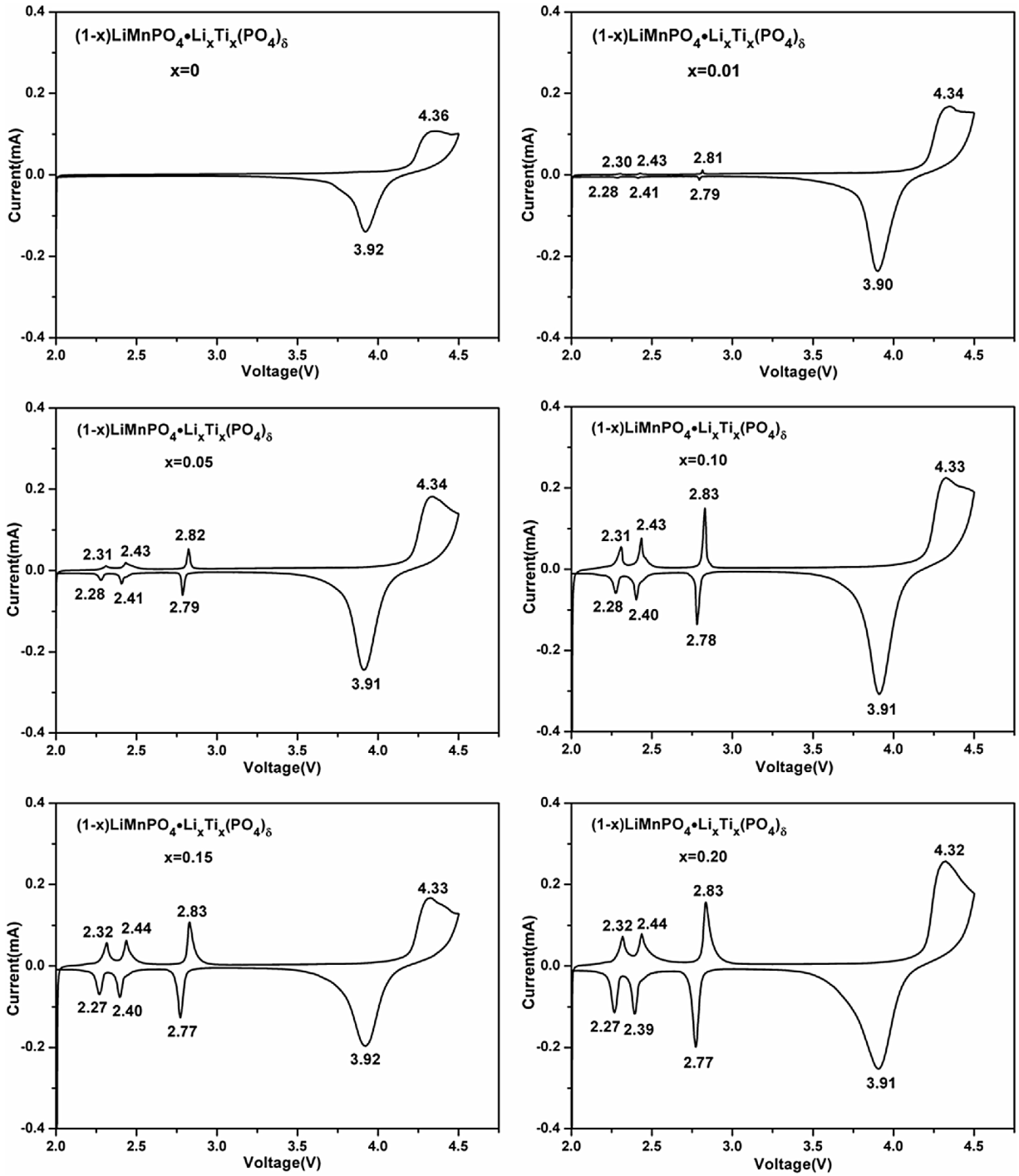

Fig. 6. Cyclic voltammetry curves of the (1-x)$LiMnPO_4{\cdot}Li_xTi_x(PO_4)_\delta$ samples.

According to Masquelier et al. [25] research, within the phosphate compositions, the potential raises from 1.5 to 2.6 V vs Li^+/Li from $LiTiPO_5$(Ti/P = 1) to TiP_2O_7 (Ti/P = 0.5), respectively. The average potential of the NASICON $LiTi_2(PO_4)_3$ materials, is located around 2.4-2.5 V vs Li^+/Li. And the surrounding around Ti^{4+}/Ti^{3+} can affect its redox potential. Hence, the two anodic peaks around 2.31 V and 2.43 V could be ascribed to TiP_2O_7; the anodic peak around 2.82 V corresponds to extract the Li^+ from $LiTi_2(PO_4)_3$ [26]. With increasing the content of Ti, the redox couple peaks that belong to titanium phosphates gradually become stronger. Therefore, it is believed that the excessive titanium tends to form TiP_2O_7 and $LiTi_2(PO_4)_3$. We can conclude that the amounts of TiP_2O_7 and $LiTi_2(PO_4)_3$ are so few that these phases aren't obvious in the XRD patterns for the samples with low content of Ti ($x \leq 0.15$); to further increase Ti content (x = 0.20), TiP_2O_7 and $LiTi_2(PO_4)_3$ phases can be observed. This well explains the phenomena in the XRD. Compared with the pure $LiMnPO_4$, the polarization of the Mn^{3+}/Mn^{2+} redox potential for the Ti additive samples slightly decreases, indicating that the Ti additive materials electrodes have an improvement in the kinetics of the lithium intercalation/deintercalation at the electrode/electrolyte interface and/or the rate of lithium diffusion in the film.

Fig. 7a shows the first charge-discharge curves of (1-x)$LiMnPO_4{\cdot}Li_xTi_x(PO_4)_\delta$ samples at 0.05 C rate. In all the cathode materials, the main charge/discharge potential plateaus around

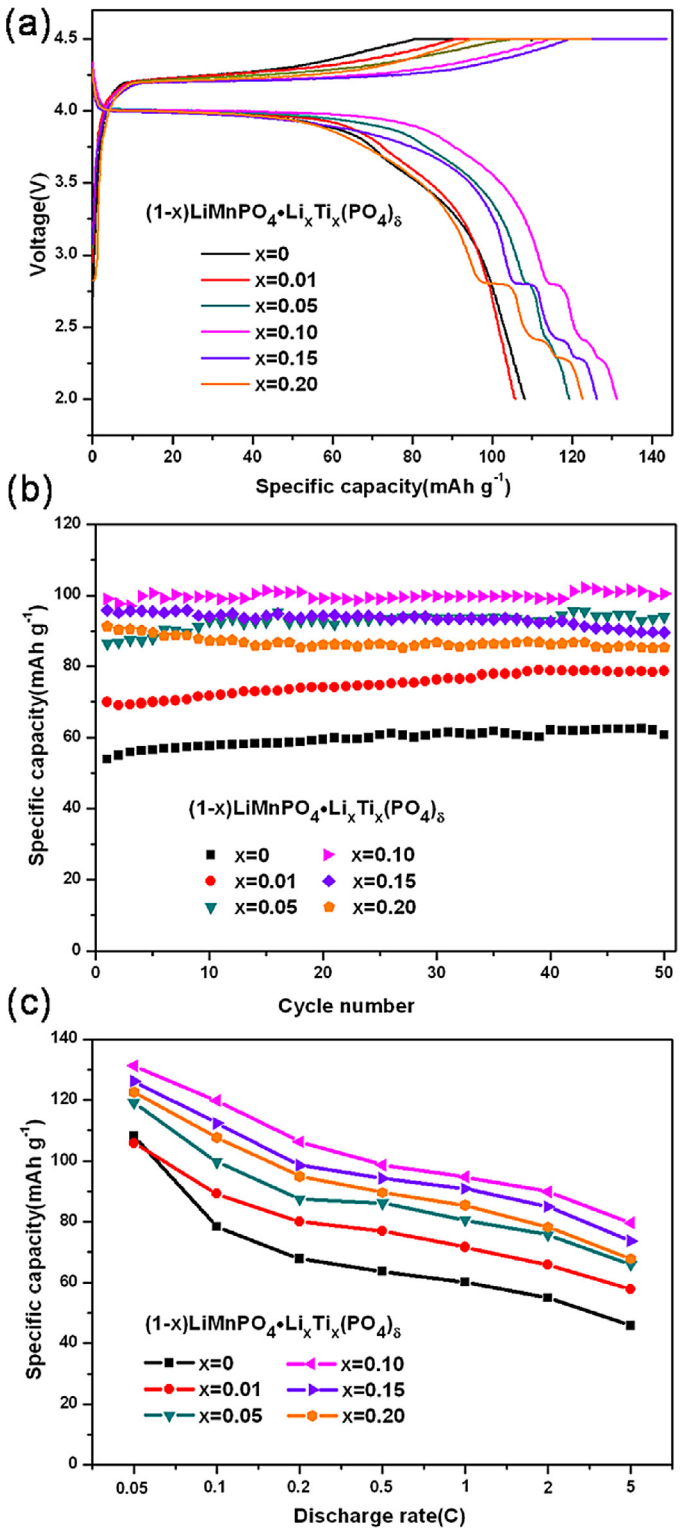

Fig. 7. (a) The first charge-discharge curves, (b) cycling performances and (c) rate capacities of the (1-x)$LiMnPO_4{\cdot}Li_xTi_x(PO_4)_\delta$ samples.

4.20/4.00 V are attributed to insert/extract of Li^+ into/from $LiMnPO_4$. For the Ti additive $LiMnPO_4$ samples except x = 0.01, there are three other plateaus around 2.79 V, 2.40 V, and 2.27 V, which should be ascribed to intercalation/deintercalation of Li^+ into/from titanium phosphates. The content of Ti is few in the x = 0.01 sample so that the three plateaus are not evident. These results are in consistent with cyclic voltammogram analysis. It can be clearly observed that the content of Ti greatly affects the electrochemical performances of the $LiMnPO_4$ samples. The specific capacity calculated in this paper is the capacity of (1-x)$LiMnPO_4{\cdot}Li_xTi_x(PO4)_\delta$ sum total. Among these samples, the x = 0.1 sample shows the highest discharge capacity of 131 mAh g^{-1} at 0.05 C rate. The initial discharge specific capacities of 126 and 122 mAh g^{-1} sequentially decrease for the x = 0.15 and x = 0.2 samples, respectively, which should be due to the low theoretical capacities of TiP_2O_7 and $LiTi_2(PO_4)_3$. As shown, the plateaus of the titanium phosphates in the samples become longer with decreasing the Mn/Ti molar ratio.

The cycling performances of all the samples are exhibited in Fig. 7b. It was measured through charging at the rate of 0.2 C and 0.5 C for discharging. It can be seen that all the samples show excellent cycle reversible capability. The discharge capacity of the pristine $LiMnPO_4$ is about 60 mAh g^{-1}, which is higher than that of the pure $LiMnPO_4$ synthesized by Hong et al. [16] using solid-state reaction. Evidently, the Ti additive cathode materials exhibit higher discharge capacity than that of pure $LiMnPO_4$. The discharge capacities for (1-x)$LiMnPO_4{\cdot}Li_xTi_x(PO_4)_\delta$ ($0 \le x \le 0.10$) show good cycling performance in 50 cycles, because there is an activated process during the cycling measurement of $LiMnPO_4$ until the capacity reaches a stable state and the quantity of titanium phosphates is little, which is not enough to impact on the cycle performance; particularly, the $LiMn_{0.90}Ti_{0.10}PO_4$ sample behaves stable cycling performance as well as the highest discharge capacity, and no capacity fade is observed even after 50 cycles; but the x = 0.15 and x = 0.2 samples exhibit relatively poor cycling performance possibly owing to the existence of much TiP_2O_7 and $LiTi_2(PO_4)_3$. The rate capacities were also tested by the following procedure: charge-discharge at the same rates of 0.05 C, 0.1 C and 0.2 C, and then followed by charging at 0.2 C and discharging with various rates of 0.5 C, 1 C, 2 C and 5 C. As shown in Fig. 7c, the discharge capacities of all the modified samples apparently exceed that of $LiMnPO_4$ at all the rates. The rate capabilities of Ti additive samples are also improved. The x = 0.1 sample exhibits better rate capability and the highest discharge capacity under various rates. Even at a high rate of 5 C, the discharge capacity of 0.9$LiMnPO_4{\cdot}Li_{0.1}Ti_{0.1}(PO_4)_\delta$ can still keep 80 mAh g^{-1}, which is approximate twice that of pristine $LiMnPO_4$. Moreover, the x = 0.01 sample shows relatively higher discharge capacities at high rates in spite of a little lower discharge capacity than the pristine $LiMnPO_4$ at low rate. From above results, it is deduced that adding appropriate amount of Ti can improve the electrochemical performance of $LiMnPO_4$. The sample synthesized with 10% Ti is considered to be the optimum.

Given the above, the 0.9$LiMnPO_4{\cdot}Li_{0.1}Ti_{0.1}(PO_4)_\delta$ sample exhibits remarkable electrochemical performance. In order to evaluate the diffusion coefficient of lithium ion, EIS tests were performed on the $LiMnPO_4$ and 0.9$LiMnPO_4{\cdot}Li_{0.1}Ti_{0.1}(PO_4)_\delta$ cathodes after 3-cycles test at 0.1 C. The Nyquist plots are shown in Fig. 8a. The spectra of $LiMnPO_4$ and 0.9$LiMnPO_4{\cdot}Li_{0.1}Ti_{0.1}(PO_4)_\delta$ show a semicircle at high-frequency region and a straight line at the low frequency. However, another semicircle appears in the high-middle frequency region for 0.9$LiMnPO_4{\cdot}Li_{0.1}Ti_{0.1}(PO_4)_\delta$, which is correlated with resistance of the SEI film. The semicircle's diameter at high-frequency region on the Z'-axis represents the charge transfer resistance (Rct). It's obvious that the charge transfer resistance of 0.9$LiMnPO_4{\cdot}Li_{0.1}Ti_{0.1}(PO_4)_\delta$ is much lower than the pure $LiMnPO_4$ sample. The straight line in low frequency represents the Warburg impedance related to Li^+ ions diffusion. The lithium ion diffusion coefficient can be calculated according to the following equation [10]:

$$D = \frac{R^2T^2}{2A^2n^4F^4C^2\sigma^2} \quad (1)$$

where R is the gas constant, T is the absolute temperature, A is the surface area of the cathode, n is the number of electrons per

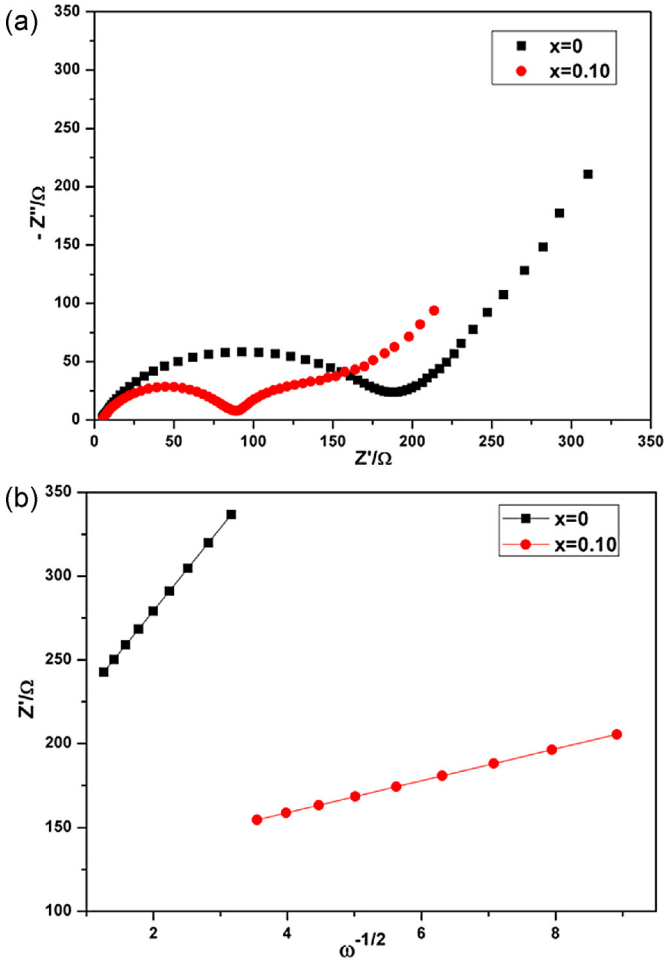

Fig. 8. (a) Electrochemical impedance spectra of $LiMnPO_4$ and $0.9LiMnPO_4{\cdot}Li_{0.1}Ti_{0.1}(PO_4)_\delta$ samples with the frequency range of 100KHz~0.01 Hz, (b) graph of Z' plotted against $\omega^{-1/2}$.

molecule attending the electronic transfer reaction, F is the Faraday constant, C is the concentration of lithium ion, D is the diffusion coefficient of lithium ion. The plots of Z' against $\omega^{-1/2}$ are shown in Fig. 8b, and σ is the slope of the straight line:

$$Z' = \sigma\omega^{-1/2} \quad (2)$$

Through calculation, the diffusion coefficient is computed to be 1.57×10^{-14} cm^2 s^{-1} for $LiMnPO_4$ and 4.24×10^{-13} cm^2 s^{-1} for $0.9LiMnPO_4{\cdot}Li_{0.1}Ti_{0.1}(PO_4)_\delta$, separately. Kang et al. [27] studied that creating a poorly crystallized layer with high Li^+ mobility like $Li_4P_2O_7$ could facilitate Li^+ transport across the surface towards the (010) facet resulting in remarkable electrochemical performance. Accordingly, titanium phosphates may be not well-crystallized with high lithium conductivity, hence, the charge transfer and lithium ion diffusion can be facilitated, which is conducive to obtain good electrochemical performance.

4. Conclusions

The $(1\text{-}x)LiMnPO_4{\cdot}Li_xTi_x(PO_4)_\delta$ (x = 0, 0.01, 0.05, 0.10, 0.15, 0.20) cathode materials have been synthesized using $CH_3COOLi{\cdot}2H_2O$, $NH_4H_2PO_4$, $(CH_3COO)_2Mn{\cdot}4H_2O$, TiO_2 nanopowders as starting materials with glucose as the carbon source and reductive agent by solid-state method. Results of the tests reveal that $LiTi_2(PO_4)_3$ and TiP_2O_7 phases exist in Ti additive $LiMnPO_4$ samples. The samples with Ti addition exhibit excellent electrochemical performance compared to the pure $LiMnPO_4$ sample. Meanwhile, the electrochemical performance is correlated with the content of Ti. The sample prepared with 10% Ti is considered to be the optimum. $0.9LiMnPO_4{\cdot}Li_{0.1}Ti_{0.1}(PO_4)_\delta$ shows the discharge specific capacity of 131 mAh g^{-1} at 0.05 C, and no capacity fade is observed even after 50 cycles at 0.5 C. The outstanding performances can be ascribed to the reduction of the grain size, the enhanced electrical conductivity and the increase of the lithium ion diffusion coefficient induced by Ti additive.

Acknowledgements

We are grateful for financial support from the Key Research Program of the Chinese Academy of Sciences (Grant No. KGZD-EW-202-4), the 973 program (Grant No. 2011CB935900), the Natural Science Foundation of Zhejiang (Grant No. Y13B030036), the Key Technology R&D Program of Ningbo (2012B10021), Ningbo Science and Technology Innovation Team (Grant No. 2012B82001).

References

[1] A.K. Padhi, K.S. Nanjundaswamy, J.B. Goodenough, Phospho-olivines as Positive-Electrode Materials for Rechargeable Lithium Batteries, J. Electrochem. Soc. 144 (1997) 1188.
[2] L. Dimesso, C. Forster, W. Jaegermann, J.P. Khanderi, H. Tempel, A. Popp, J. Engstler, J.J. Schneider, A. Sarapulova, D. Mikhailova, L.A. Schmitt, S. Oswald, H. Ehrenberg, Developments in nanostructured $LiMPO_4$ (M = Fe, Co, Ni, Mn) composites based on three dimensional carbon architecture, Chem. Soc. Rev. 41 (2012) 5068.
[3] Z.L. Gong, Y. Yang, Recent advances in the research of polyanion-type cathode materials for Li-ion batteries, Energy Environ. Sci. 4 (2011) 3223.
[4] C. Delmas, Maccario, M. Maccario, L. Croguennec, F. Le Cras, F. Weill, Lithium deintercalation in $LiFePO_4$ nanoparticles via a domino-cascade model, Nat. Mater. 7 (2008) 665.
[5] X.L. Wu, L.Y. Jiang, F.F. Cao, Y.G. Guo, L.J. Wan, $LiFePO_4$ Nanoparticles Embedded in a Nanoporous Carbon Matrix: Superior Cathode Material for Electrochemical Energy-Storage Devices, Adv. Mater. 21 (2009) 2710.
[6] H. Song, K.T. Lee, M.G. Kim, L.F. Nazar, J. Cho, Recent Progress in Nanostructured Cathode Materials for Lithium Secondary Batteries, Adv. Funct. Mater. 20 (2010) 3818.
[7] A. Yamada, S.C. Chung, K. Hinokuma, Optimized $LiFePO_4$ for lithium battery cathodes, J. Electrochem. Soc. 148 (2001) A224.
[8] P.R. Kumar, M. Venkateswarlu, M. Misra, A.K. Mohanty, N. Satyanarayana, Carbon Coated $LiMnPO_4$ Nanorods for Lithium Batteries, J. Electrochem. Soc. 158 (2011) A227.
[9] S. Oh, S. Oh, C. Yoon, B. Scrosati, K. Amine, Y. Sun, High-Performance Carbon-$LiMnPO_4$ Nanocomposite Cathode for Lithium Batteries, Adv. Funct. Mater. 20 (2010) 3260.
[10] J. Liu, X. Liu, T. Huang, A. Yu, Synthesis of nano-sized $LiMnPO_4$ and in situ carbo n coating using a solvothermal method, J. Power Sources 229 (2013) 203.
[11] T. Drezen, N. Kwon, P. Bowen, I. Teerlinck, M. Isono, I. Exnar, Effect of particle size on $LiMnPO_4$ cathodes, J. Power Sources 174 (2007) 949.
[12] N. Kwon, T. Drezen, I. Exnar, I. Teerlinck, M. Isono, M. Graetzel, Enhanced Electrochemical Performance of Mesoparticulate $LiMnPO_4$ for Lithium Ion Batteries, Electrochem. Solid-State Lett. 9 (2006) A277.
[13] D. Choi, D. Wang, I. Bae, J. Xiao, Z. Nie, W. Wang, V.V. Viswanathan, Y.J. Lee, J. Zhang, G.L. Graff, Z. Yang, J. Liu, $LiMnPO_4$ Nanoplate Grown via Solid-State Reaction in Molten Hydrocarbon for Li-Ion Battery Cathode, Nano Lett 10 (2010) 2799.
[14] Z. Qin, X. Zhou, Y. Xia, C. Tang, Z. Liu, Morphology controlled synthesis and modification of high-performance $LiMnPO_4$ cathode materials for Li-ion batteries, J. Mater. Chem. 22 (2012) 21144.
[15] D. Wang, C. Ouyang, T. Drézen, I. Exnar, A. Kay, N. Kwon, P. Gouerec, J.H. Miners, M. Wang, M. Grätze, Improving the Electrochemical Activity of $LiMnPO_4$ Via Mn-Site Substitution, J. Electrochem. Soc. 157 (2010) A225.
[16] J. Hong, F. Wang, X. Wang, J. Graetz, LiFexMn1-xP.O4., A cathode for lithium-ion batteries, J. Power Sources 196 (2011) 3659.
[17] H. Fang, H. Yi, C. Hu, B. Yang, Y. Yao, W. Ma, Y. Dai, Effect of Zn doping on the performance of $LiMnPO_4$ cathode for lithium ion batteries, Electrochim. Acta 71 (2012) 266.
[18] T. Shiratsuchi, S. Okada, T. Doi, J. Yamaki, Cathodic performance of $LiMn_{1-x}M_xPO_4$ (M = Ti, Mg and Zr) annealed in an inert atmosphere, Electrochim. Acta 54 (2009) 3145.
[19] J. Lee, M. Park, B. Anass, J. Park, M. Paik, S. Doo, Electrochemical lithiation and delithiation of $LiMnPO_4$: Effect of cation substitution, Electrochim. Acta 55 (2010) 4162.
[20] G. Yang, H. Ni, H. Liu, P. Gao, H. Ji, S. Roy, J. Pinto, X. Jiang, The doping effect on the crystal structure and electrochemical properties of $LiMn_xM_{1-x}PO_4$ (M = Mg, V, Fe, Co, Gd), J. Power Sources 196 (2011) 4747.

[21] S. Wu, M. Chen, C. Chien, Y. Fu, Preparation and characterization of Ti^{4+}-doped $LiFePO_4$ cathode materials for lithium-ion batteries, J. Power Sources 189 (2009) 440.
[22] L. Li, X. Li, Z. Wang, L. Wu, J. Zheng, H. Guo, Stable cycle-life properties of Ti-doped $LiFePO_4$ compounds synthesized by co-precipitation and normal temperature reduction method, J. Phys. Chem. Solids 70 (2009) 238.
[23] Z. Wang, Q. Pang, K. Deng, L. Yuan, F. Huang, Y. Peng, Y. Huang, Effects of titanium incorporation on phase and electrochemical performance in $LiFePO_4$ cathode material, Electrochim. Acta 78 (2012) 576.
[24] S. Chung, J.T. Bloking, Y. Chiang, Electronically conductive phospho-olivines as lithium storage electrodes, Nat. Mater. 1 (2002) 123.
[25] S. Patoux, C. Masquelier, Lithium Insertion into Titanium Phosphates, Silicates, and Sulfates, Chem. Mater. 14 (2002), 5057.
[26] L. Liu, M. Zhou, G. Wang, H. Guo, F. Tian, X. Wang, Synthesis and characterization of $LiTi_2(PO_4)_3$/C nanocomposite as lithium intercalation electrode materials, Electrochim. Acta 70 (2012) 136.
[27] B. Kang, G. Ceder, Battery materials for ultrafast charging and discharging, Nature 458 (2009) 190.